Probe Molecule Spectroscopy of NaCl Aerosol Particle Surfaces

Ephraim Woods III,* Stephen F. Morris, Carl N. Wivagg, and Lauren E. Healy

Department of Chemistry, Colgate University, 13 Oak Drive, Hamilton, New York 13346

Received: July 10, 2005; In Final Form: October 4, 2005

Excited-state absorption spectroscopy and ionization threshold measurements for coumarin 314 (C314) adsorbed to the surface of NaCl aerosols characterize the chemical environment of the particle surface as a function of relative humidity (RH). An atmospheric pressure flow of aerosol passes through an ionization cell where two-photon laser ionization of the adsorbed molecules produces a net charge on the particle. Monitoring this charge as a function of the laser wavelength produces either the absorption spectrum of the $S_1 \leftarrow S_0$ transition or the ionization threshold. The wavelength of maximum absorption for the S_1 excited-state shifts from 448 nm for RH $<$ 5% to 441 nm for RH $=$ 60%, indicating that adsorbed water decreases the polarity of the surface. Similarly, the ionization threshold increases from 5.10 to 5.27 eV over a similar range of RH. The decrease in polarity is attributable to changes in the local electric field experienced by C314, which is on the order of 1×10^7 V/cm, and is correlated with changes in the surface topography. Using a continuum model, we estimate the contributions to the measured thresholds of the polarization response of the surface ions and the electric field and calculate an effective dielectric constant for the adsorbed water film. For a multilayer water coverage (RH $=$ 65%), the effective dielectric constant is approximately 2.4. These results demonstrate that the changes in surface topography with adsorbed water are as important as direct water−solute interactions in determining the solvent character of the surface.

I. Introduction

Aerosol particles play an important role in the chemistry of the troposphere, acting as both catalytic surfaces and as sources of reactive species. Sea salt particles, in particular, are important sources of highly reactive halogen atoms in the atmosphere. Wave action in the ocean creates these particles as aqueous droplets, but they may also exist as crystalline particles at low relative humidity (RH) or as reverse micelles.[1,2] The morphology,[3] heterogeneous chemistry,[4] and optical properties[5] of NaCl particles are strongly dependent on the amount of water associated with the particle. Considering the effect of adsorbed water on NaCl surfaces is crucial to understanding their chemistry.

Surface-adsorbed water on NaCl aerosol particles is difficult to characterize spectroscopically because of competing signals that arise from liquid water pockets within the particle.[3,6] However, water adsorbed to the surface of single-crystal NaCl has been well-studied using infrared (IR) spectroscopy[7,8] and atomic force microscopy (AFM).[9,10] The IR results reveal the integrated coverage of adsorbed water as a function of RH, and the AFM results show that water preferentially adsorbs to step edges causing the smoothing and, ultimately, the movement of the steps themselves. Water adsorption isotherms on NaCl crystallites[11] imply greater water coverage compared to the single crystal at low water vapor pressures, which can be attributed to the large defect density of the films. These experimental results, together with Monte Carlo simulations,[12] produce a detailed picture of water adsorbed to NaCl surfaces.

Our goal is characterize how adsorbed water and the associated topographical changes alter the chemical environment for molecules adsorbed to the surface of NaCl. In particular, we want to characterize the solvating capacity of this unique and asymmetric chemical environment. Field studies show that, in addition to water, sea salt particles play host to a wide variety of organic molecules, of both biological and anthropogenic origin.[13] Solvent effects on the rates of chemical reactions are often drastic; therefore, characterizing the solvent environment of molecules adsorbed to NaCl surfaces should yield some insight into the chemistry that takes place there.

Chemists usually cast the solvation capacity of a medium in terms of its polarity. The concept of polarity encompasses the entire range of specific and nonspecific perturbations of a solute by its environment, excluding only those that result in chemical changes. Polarity is most often used qualitatively, but a number of quantitative empirical polarity scales exist.[14] One generally useful approach to assessing polarity is to measure the wavelength of maximum absorption (λ_{max}) for electronic transitions in solvatochromic probe molecules. Alternatively, in cases where the polarization response of the solvent dominates specific dipolar interactions, the static dielectric constant is a useful measure of solvation capability. For example, continuum dielectric models such as the Born equation describe the photoionization threshold energy (IE) of molecules dissolved in many nonpolar liquids.[15−19] Though most often applied to homogeneous solvents, both λ_{max}[20,21] and IE[22,23] measurements have been used successfully to describe the chemical environment of the liquid water surface. Further, IE measurements have been used to characterize the surface TiO_2 electrodes as well.[24]

The present work makes use of both λ_{max} and IE measurements to uncover the factors that control polarity for NaCl aerosol surfaces. These experiments are complementary. The λ_{max} values are useful in establishing trends and making connections with bulk solvents. Because ground-state ions lend themselves to computational descriptions much better than do excited states, the IE measurements enable the use of continuum models to assess the polarization response separately from other

* Corresponding author. E-mail: ewoods@mail.colgate.edu.

10.1021/jp0537916 CCC: $30.25
Published on Web 11/05/2005

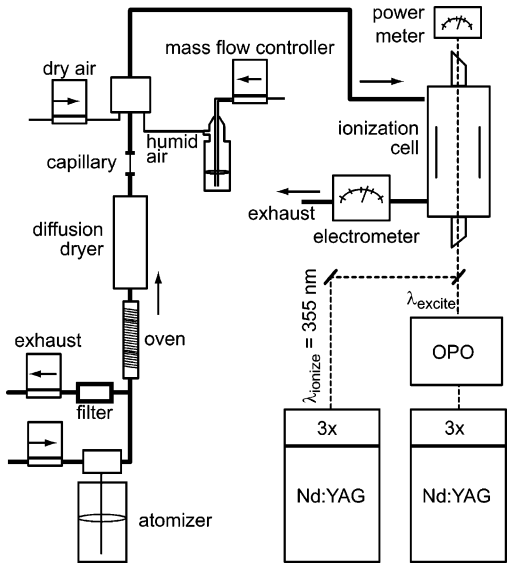

Figure 1. Schematic diagram of the experimental apparatus. The arrows indicate the direction of flow. The excited-state spectroscopy experiments use both laser systems, and the ionization threshold experiments use only the tunable Nd:YAG pumped OPO.

interactions. Our experimental method, described in detail in the following section, combines the sensitivity of laser-ionization detection with ambient pressure flows, making it straightforward to alter RH. Coumarin 314 (C314), the probe molecule for our experiment, is a highly solvatochromatic molecule that has been used to characterize surfaces in the past.[20] It also has a low ionization potential (7.1 eV in the gas phase[25]) making it particularly suitable for our method.

II. Experimental Section

The experimental method is based on the photoelectric charging of aerosols.[26−28] The operating principle is that, when ionizing radiation encounters a particle, photoelectrons may be liberated from the particle's surface, leaving a net positive charge on the aerosol. Even at atmospheric pressure, the mean free path of the near-threshold photoelectrons is sufficiently large that the probability that the photoelectron recombines with the particle is small. An electrometer measures the positive charge in the particle stream allowing for sensitive detection of low-ionization-potential species on the surface of an aerosol particle. Ultraviolet light from a lamp is the usual ionization source. This technique is used in portable devices designed to detect trace polycyclic aromatic hydrocarbons[27] as well as in the laboratory setting to monitor desorption kinetics.[29] Our experiment differs from the traditional version in that tunable lasers replace the UV lamp, allowing for the measurement of both the ionization threshold and excited-state spectroscopy of adsorbed molecules.

We produce aerosol particles from an aqueous, 295 K source solution of 5×10^{-2} M NaCl and 2×10^{-6} M C314 made from distilled, deionized water. Figure 1 shows a schematic illustration of the experiment. An atomizer (TSI model 3075) produces a 2.0 standard liter-per-minute (slpm) flow of air containing a large number density of aqueous droplets from the source solution. Filters remove organic impurities and particulate matter from the carrier air before using it to generate particles. To guarantee that the particles are crystalline over the whole range of RH used in this study, we dry them to below 10% RH and then adjust to a higher RH when desired. Dried particles also equilibrate with water vapor more quickly than do supersaturated aqueous droplets,[3] further making this particle preparation scheme attractive.

The first stage of the flow system divides the stream in a 10:1 ratio, with the larger flow exiting the system through an exhaust. A capillary tube in the low-flow line produces this large ratio, and a mass flow controller in the exhaust line regulates the flows. Splitting the flow makes drying the particles easier and avoids photoelectron recombination processes that occur at large particle number densities.[30] The smaller, 0.2 slpm flow passes through a 390 K oven and a diffusion dryer to remove the water solvent. The resulting crystalline particles are predominantly NaCl covered with approximately 50 C314 probe molecules. This level of coverage effectively excludes interactions between probe molecules. The mean final particle mobility diameter is near 75 nm, and the geometric standard deviation is approximately 1.8, both estimated using data from the manufacturer. Repeating the experiment with 150 nm mean diameter particles results in slightly lower signals owing to the greater probability of geminate photoelectron recapture,[31] but there is no significant change in the measured quantities.

The next stage of the flow system dilutes the aerosol flow to 2.2 slpm using a mixture of dry air and air that is bubbled through water. Controlling the relative amount of dry and humid air tunes the RH, which we monitor using a traceable hygrometer near the outlet of the ionization cell. The measured RH is generally within 10% of the value calculated on the basis of flows but fluctuates by as much as 5% during a given experiment. The dry dilution air passes trough a Po-210 static control ionizer (NRD), producing equal concentrations of positively and negatively charged air molecules and bringing the aerosol particles into charge equilibrium through collisions. The interaction time of the water vapor with particles prior to analysis is approximately 5 s. Increasing the total flow to 3.2 slpm reduces the residence time of particles in the system by ∼50% but leaves our results unchanged. We conclude that the particles are in equilibrium (or nearly so) with the water in the carrier gas.

The aerosol flow then interacts with tunable laser light in an ionization cell. The laser(s) photoionize the probe molecules, and the nascent photoelectrons precipitate out in a small (5 V/cm) electric field. The field is too small to alter the particle trajectories or significantly perturb the spectroscopy. In the ionization threshold experiments, either a single ultraviolet photon or two visible photons from the same laser pulse ionize the probe molecule in the threshold energy region. A frequency tripled, 10-Hz Nd:YAG (Spectra Physics) pumps an OPO (OPOtek) to generate the visible light (450−520 nm) for the two-photon ionization. Frequency doubling this light in BBO produces the ultraviolet radiation for the single-photon ionization. The line width of the visible radiation is approximately 20 cm^{-1}, and we typically use powers in the range 5−10 mJ/pulse. For the two-photon experiment, the laser focuses loosely (∼1 mm diameter) in the center of the ionization cell. In the single-photon experiment, the laser passes through the cell unfocused, with a beam diameter of 3 mm. Following the ionization of the probe molecules, the aerosols carry a net positive charge. Scanning the ionization laser's wavelength while monitoring the charge in the aerosol stream using an aerosol electrometer (TSI) produces the aerosol photoionization spectrum from which we extract the threshold value. We refer to this threshold as the ionization threshold, but it is possible that ionization processes that produce charge pairs on the surface occur at lower energies. This experiment is sensitive only to ionization events that result in the emission of electrons from the particle.

In the excited-state spectroscopy experiments, a tunable visible photon prepares the excited electronic state and a second, fixed-frequency photon ionizes only the electronically excited molecules. In this case, scanning the excitation laser while monitoring the ionization signal produces a spectrum that reflects the excited-state absorption spectrum. The tunable laser is the same Nd:YAG-pumped OPO as above, but operating at only 1 mJ/pulse to suppress multiphoton ionization. The ionization laser is the third harmonic (355 nm) of a separate 10 Hz Nd:YAG laser (Spectra Physics). We typically use 1 mJ/pulse from this laser. These beams overlap in time and copropagate unfocused through the ionization cell with a 3 mm beam diameter.

In both experiments, small manual adjustments of an iris near the output of the OPO hold the power of the tunable laser constant during the scans. These adjustments do not affect the beam diameter in the ionization cell, which is roughly 2 m from the iris. A miniature fiber optic spectrometer (Ocean Optics) measures the laser wavelength using diffuse reflections from optics. For each data point in a scan, the data collection software (LabView) averages the signal for 2 s (20 laser shots). A 3 s pause in data collection between changing the wavelength of the laser and signal averaging ensures that the particles ionized at the new wavelength have ample time to reach the electrometer before signal averaging begins.

III. Morphology of NaCl Aerosols

Studying aerosol particles rather than bulk materials makes the results more relevant to atmospheric problems. A challenging aspect of using aerosols, though, is that the morphology of the particles is strongly dependent on the conditions and difficult to characterize. For example, NaCl aerosol particles exhibit a hysteresis effect with changing RH. The deliquescence point, where water vapor is in equilibrium with saturated aqueous droplets, is 75% RH (similar to the thermodynamic value), whereas the point where aqueous droplets crystallize upon decreasing RH is 44%. Whether a particular particle is crystalline at values of RH between 44% and 75%, then, depends on its history. As mentioned above, we dry the particles below 44% RH prior to adjusting the final RH; therefore, all of the particles in our experiments should be crystalline.

Another important issue of morphology is the amount and structure of surface-adsorbed water as a function of RH for crystalline particles. Previous work using infrared spectroscopy[3,6] shows that aerosol particles produced from atomized solutions contain an anomalously large amount of water at values of RH below the deliquescence point. Pockets of aqueous water trapped within the particle account for this observation. Although the particles used here are smaller than the ones used in ref 3 (75 nm vs 300 nm), similar pockets of water may exist within our particles. Even if they are present, they have no impact on our data. The data presented here are sensitive to changes in RH, indicating empirically that these data are representative of surface sites. Unfortunately, the large volume of trapped water makes quantifying the surface adsorbed water for aerosol particles difficult. In this work, we rely on literature data concerning water adsorbed to the surface of single-crystal NaCl and NaCl crystallites to develop reasonable expectations about the surface morphology of the particles in this experiment.

Ewing and co-workers determine coverage (Θ) values for water on the freshly cleaved NaCl (100) surface[32] using infrared spectroscopy. They identify four separate domains of coverage: a low-coverage region ($\Theta < 0.5$) characterized by islands of hydrogen-bonded water molecules, a transition region ($0.5 < \Theta < 2.5$) where coverage increases very rapidly with increasing pressure, a high-coverage region ($2.5 < \Theta < 3.5$) associated with a liquidlike multilayer, and a presolution region ($\Theta > 3.5$) immediately preceding the deliquescence point. Barraclough and Hall[11] used IR to measure water adsorption isotherms onto crystallites of NaCl. Interestingly, isotherms for single-crystal surfaces and crystallite films are very similar for RH > 40%. The similarity between these two data sets, along with the consistency in the deliquescence point among particles and bulk materials, suggests that above some critical value of RH, single-crystal and thin film surfaces are similar. Using AFM, Salmeron and co-workers[9,10] show that, above 40% RH, the surface dissolution of both cations and anions leads to rapid topography changes and the rounding of defect sites. In this regime, the distinction between single-crystal and rough surfaces is naturally less important. Further, the point of transition between slow and fast topographical changes corresponds closely to $\Theta = 1$ in the single-crystal adsorption isotherm (~38% RH), thus water−water interactions rather than water−NaCl interactions govern adsorption beyond this point. Below 40% RH, the integrated coverage is generally greater for rough surfaces than single crystals, and topographical changes occur much more slowly. Because water adsorption is enhanced at defect sites,[10] the greater defect density in the NaCl film accounts for the enhancement in coverage. We expect that the situation is similar with aerosol particles, whose defect density is unknown. The greatest uncertainty in generalizing these results to aerosol particles, then, is the water coverage for RH < 40%. At higher values, the literature isotherms should be applicable.

Using these observations as a guide, we generate a description of the aerosol surfaces at the values of RH used in our experiments. Below 5% relative humidity, there is very sparse water adsorbed mainly to defect sites. The NaCl surface, itself, is rough and not significantly changed by water. At a target RH of 15−20%, the integrated coverage is a significant fraction of a monolayer, but still concentrated on defect sites. For the RH range 40−50%, we expect coverage similar to the transition region described for the single crystal. A small fraction of the surface ions are mobile (1% at RH = 40%), and topographical changes are evident. Last, for 60−70% RH, we expect the particles have a liquidlike multilayer water film. The underlying lattice undergoes rapid step displacement and rounding of edges.

One final issue is the location of the C314 probe molecules. As mentioned above, the observation that our results depend on RH, and thus, the amount of adsorbed water, strongly suggests the results are indicative of primarily surface-adsorbed C314. C314 has a low solubility in water (1.5×10^{-5} M at 20 °C) and is likely surface active. When the aqueous droplets crystallize during the drying stage of the experiment, the volume of the particle is more than 100 times smaller than the initial droplet, and the solubility of C314 is exceed by a factor of approximately 10. It makes sense, then, that only a small fraction of the molecules can be trapped inside the crystal; however, the surface adsorbed molecules are not necessarily isolated. Using initial concentrations of C314 near saturation results in noticeably broadened and red-shifted spectra, and we attribute the changes to aggregates of C314 on the surface of the crystal. In practice, we use initial concentrations of 2×10^{-6} M, which is comfortably below the onset for aggregation but still produces a strong signal.

IV. Results

Excited-State Spectroscopy. The $S_1 \leftarrow S_0$ spectroscopy of C314 is subject to both solvatochromic shifts associated with the polarizability and dipolar character of the solvent environ-

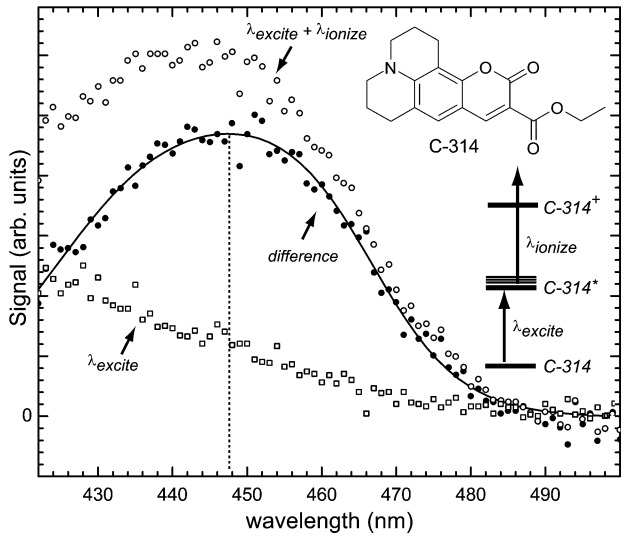

Figure 2. Electronic spectroscopy of the $S_1 \leftarrow S_0$ transition for C314 adsorbed to the surface of NaCl aerosols: (○) combined signal of both excitation and ionization lasers; (□) just background signal from the excitation laser; (●) difference of the two. The RH is <5% for these data and the value of λ_{max} is 448 nm.

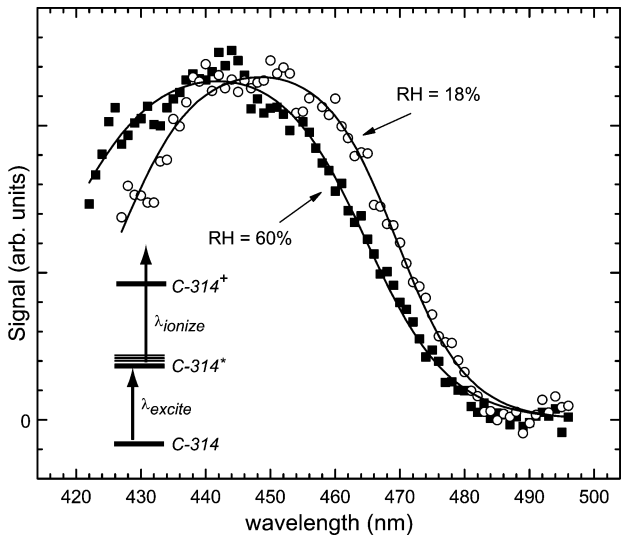

Figure 3. Comparison of the electronic spectroscopy of the $S_1 \leftarrow S_0$ transition for C314 adsorbed to the surface of NaCl aerosols at RH = 18% and RH = 60%. The value of λ_{max} changes from 448 to 441 nm over this range of RH.

ment and electrochromic shifts attributable to electric fields at the surface generated by the Na^+ and Cl^- ions. Because the S_1 state of C314 has a larger dipole moment than the ground state ($|\Delta\mu| \sim 4$ D), the solvent stabilization energy is greater for the excited state and the value of λ_{max} shifts to longer wavelengths with increasing polarity of the solvent (positive solvatochromatism). For C314, λ_{max} ranges from 418 nm for nonpolar solvents such as cyclohexane to 448 for strongly polar solvents, like water.

Figure 2 shows the results of the excited-state spectroscopy experiment for C314 adsorbed to NaCl aerosol particles with RH < 5%. We refer to this condition as "dry", although there is undoubtedly some water on the surface. Both the excitation and ionization lasers by themselves produce a background signal attributable to multiphoton ionization. Figure 3 shows the total two-laser signal, the wavelength-dependent background from the excitation laser, and the difference between the two. The background signal owing to the ionization laser is a constant

TABLE 1: Summary of Excited-State Spectroscopy and Ionization Threshold Data

% RH	Θ	λ_{max} (nm)	IE (eV)	ϵ_{eff}
<5		448 ± 0.3	5.10 ± 0.02	1.0
15−20	<1	448 ± 0.3	5.11 ± 0.02	1.0
40−50	1−2.5	445 ± 0.5	5.17 ± 0.02	1.4
60−70	2.5−3.5	441 ± 0.7	5.27 ± 0.03	2.4

throughout the scan. The difference spectrum has contribution from only the two-laser process where C314 must first be electronically excited to be ionized; therefore, it represents the electronic absorption spectrum of the C314. To avoid bias in assigning the wavelength of maximum absorbance, λ_{max}, we fit the difference spectrum using an arbitrary functional form that represents the shape of the spectrum well and use the maximum of the fitted curve. For the dry NaCl aerosol data shown in Figure 3, the λ_{max} value is 448 nm, similar to that for C314 dissolved in pure water. In qualitative terms, the NaCl aerosol surface is a polar environment.

The static dielectric constant for NaCl of 5.9 is indicative of the polarizability of the ions. Molecular liquids with dielectric constants similar to those for NaCl (like glacial acetic acid, 6.1, and *p*-chlorotoluene, 5.9) have λ_{max} values near 335 nm for C314. If the polarizability of the NaCl surface were the dominant solvent effect on the C314 spectroscopy, the λ_{max} value would be near 335 nm. Instead, the λ_{max} value for the NaCl aerosol surface is 448 nm. This large disparity suggests that the high polarity of the dry NaCl aerosol surface is attributable to ion-dipole forces between the surface and C314 and not to the polarizability of the surface.

Table 1 lists the values of λ_{max} determined from the fits for four values of RH, and Figure 3 compares the results of this experiment for RH = 18% and RH = 60%. For reference, Table 1 includes the approximate values for coverage, Θ, deduced from literature data.[32] The uncertainties represent one standard deviation for multiple trials with similar values of RH. Clearly, as the RH increases, the value of λ_{max} decreases. In going from the dry particle to 60% RH, λ_{max} decreases by 7 nm, which is an increase of 44 meV in photon energy and represents nearly 20% of total range. The majority of the shift occurs for RH > 40%. This trend indicates that adsorbed water reduces the polarity of the NaCl surface, a counterintuitive result given that water is a very polar solvent. The addition of a polar solvent in the neighborhood of the C314 should provide additional solvent capacity. However, water can alter the electric field generated by the NaCl lattice, leading to the observed blue shift. One mechanism for water to change the field experienced by C314 is to generate a field that opposes that of the salt, as should happen for a dielectric material. This effect may be small as the water molecules do not necessarily lie between C314 and the surface. An additional possibility is that the rearrangement of the ions in the vicinity of the probe molecule accounts for the changes in the electric field.

This latter interpretation is consistent with previous findings from AFM experiments.[10] Certainly, the movement of ions does not play a role on the time scale of electronic excitation. However, the ability of the adsorbed water to change the topography of the surface through ion motion may have a large impact on the electric field experienced by C314, and such an effect would be most pronounced on defect sites. Furthermore, the mobility of the ions increases drastically above 40% RH, so the changes in λ_{max} are well-correlated with the onset of this rapid ion mobility. By invoking the changes in defect sites to explain these observations, we imply that our results pertain to

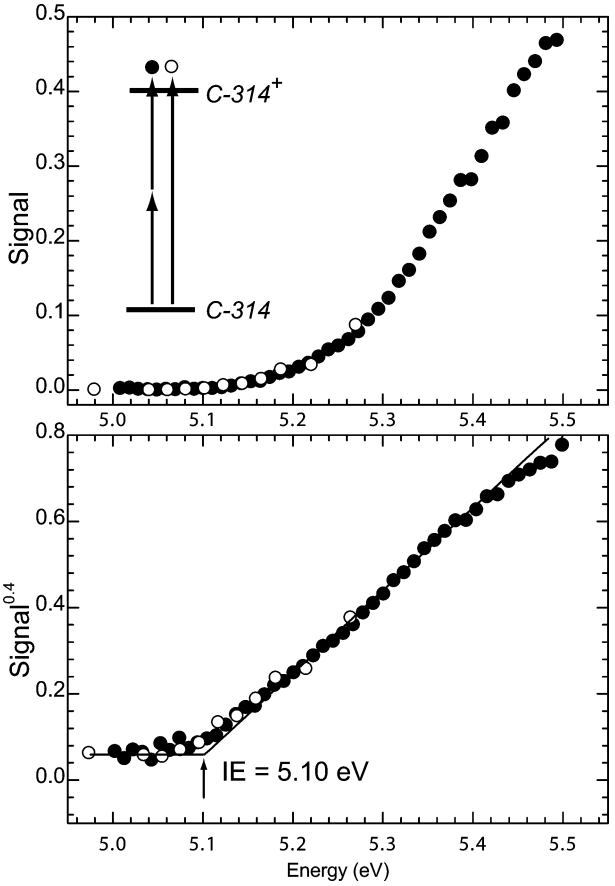

Figure 4. Ionization threshold measurement for C314 adsorbed to the surface of NaCl aerosol particles. The top frame shows the raw signal for both the single-photon ionization (open circles) and two-photon ionization (closed circles). The bottom frame shows the same data plotted as signal$^{0.4}$ vs photon energy. The measured threshold is 5.10 eV.

C314 molecules adsorbed to those sites, and a later section addresses this assertion in more detail.

Though we would not conclude that dipole interactions between the water and C314 are absent, they are not the dominant factor controlling the chemical environment of the C314. The major effect of the water is a secondary one, its effect on the salt itself and the field experienced by C314. Consequently, the observed effect may apply quite generally to other adsorbed organic molecules. These results also indicate that C314 remains adsorbed to the NaCl surface at all values of coverage studied here. Benderskii and Eisenthal[20] measured the spectroscopy of C314 at the air−water interface and found the value of λ_{max} to be 425 nm. Even at RH = 60%, our λ_{max} value is 441 nm, clearly different than for the air−water interface.

Ionization Thresholds. The top panel of Figure 4 shows a photoionization spectrum normalized to 1.0 mJ/pulse, for C314 adsorbed to nominally dry NaCl aerosol particles (<5% RH) using the two-photon ionization scheme in Figure 4. The typical way to extract ionization thresholds from photoionization yield experiments is to use a power law description of the signal. An often-used empirical form for the photoionization yield, Q, is

$$Q(E_{h\nu}) \propto (E_{h\nu} - \mathrm{IE})^{2.5} \quad (1)$$

where $E_{h\nu}$ is the energy of the ionizing radiation and IE is the threshold energy. This form has been used to analyze near-threshold photoconductivity spectra in bulk nonpolar liquids[15,16,19,33] and photoionization spectra at the surface of liquid water.[23] A plot of $Q^{0.4}$ vs $E_{h\nu}$ is linear in the near-threshold energy region, and the threshold energy is the x-intercept of the linear portion of the plot.

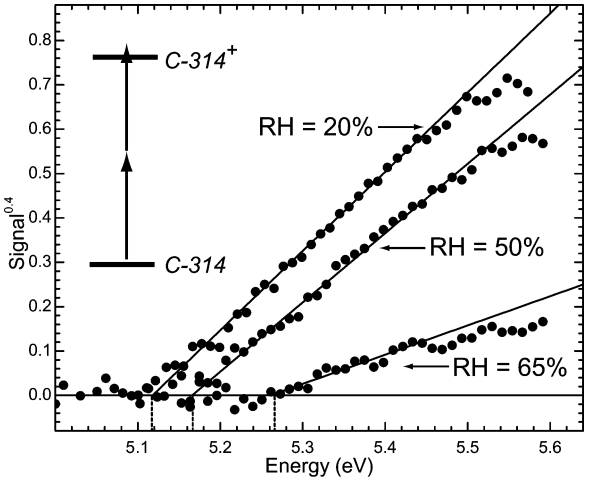

Figure 5. Comparison of the ionization threshold data for three values of RH. The nonzero baseline for each of these data sets has been subtracted away. The measured thresholds are 5.11, 5.17, and 5.27 eV for 20%, 50%, and 65% RH, respectively.

The bottom panel of Figure 5 shows the raw data in Figure 2 plotted as $Q^{0.4}$ vs $E_{2h\nu}$ for our two-photon ionization scheme. The signal below threshold for two-photon ionization is not zero because there is some probability of three-photon or higher-order processes at wavelengths below threshold. As a result, we regress the linear portion of the signal to the baseline implied by the background signal rather than to zero. The threshold measured this way is 5.10 eV, which is about 1.8 eV lower than the threshold for gas-phase C314. This change is large but not without precedent. A similarly large change in ionization threshold has been observed for dye molecules adsorbed to the surface of TiO_2 electrodes.[24] The calculated thresholds are independent of laser power above a critical value, which is typically near 3−4 mJ/pulse. Below this critical value, the measured thresholds are higher, perhaps because of vibrational relaxation of the S_1 state in the two-photon process. To ensure that this two-photon method produces the real threshold, we repeat selected experiments using single-photon ionization. Figure 4 also shows the results from the single-photon ionization experiment, and the measured threshold is identical within error to the one measured using the two-photon scheme. Currently, the single-photon experiment requires the manual tuning of nonlinear crystals and is prohibitively time-consuming; therefore, in practice, we use the two-photon scheme almost exclusively.

Table 1 summarizes the IE data and Figure 5 shows the ionization threshold results for RH ranging from <5% to 65%. For clarity, Figure 5 shows each of the traces with their baseline signals subtracted out. The ionization threshold grows monotonically with increasing coverage of water molecules from 5.10 eV for RH < 5% to 5.27 eV for RH = 65%, an increase of 0.17 eV. The trend in the ionization potential data is consistent with the electronic spectroscopy. There is little change in threshold at the lowest value of RH, and the majority of the change occurs for RH > 40%. It is difficult to account for the RH dependence by considering the direct effect of the adsorbed water. Water is among the most polar solvents and C314−water interactions would be expected to lower the ionization threshold rather than raise it. Instead, this trend is again attributable to changes in the electric field experienced by the C314. It is well-established that applied electric fields lower the ionization potential of atomic and molecular species (a Stark shift), and

methods such as ZEKE-PFI exploit it to great utility in ion spectroscopy.[34] In this case, the electric field is supplied by the substrate and modified by the addition of adsorbed water.

Estimation of the Polarization Response. A useful way to understand quantitatively the ionization threshold data is to compare our measured thresholds to the gas-phase value. First, consider only the case of the "dry" NaCl aerosol results. We relate the threshold for surface-bound molecules to the gas-phase threshold with the equation,

$$\mathrm{IE}_{\mathrm{surf}} = \mathrm{IE}_{\mathrm{gas}} + P^{+} + S \qquad (2)$$

where P^+ represents the polarization response of the surroundings to the creation of an ion and S represents the Stark shift. Dividing the total stabilization energy into continuum (P^+) and discrete (S) terms enables the use of continuum models to estimate the individual contributions and provide insight into the environment of the C314 probe molecule.

One such description is the Born equation, which has been used successfully to understand ionization thresholds of solutes in nonpolar liquids.[15,16,19] This model treats the solvent cavity as a sphere embedded in a uniform dielectric. Another model is the conductor polarizable continuum model (CPCM)[35,36] as implemented in the Gaussian 03 suite of programs.[37] This model has the benefit of treating the shape of the molecule explicitly and implicitly accounting for changes in the molecular dipole moment upon ionization. As with the Born equation, the principle parameter in this model is the dielectric constant of the surrounding "solvent". Because we measure threshold values and not vertical ionization potentials, and because there is little expected change in the equilibrium geometry of C314 or the underlying NaCl lattice upon ionization, our measured threshold for the dry surface should correspond more closely to the adiabatic threshold than the vertical value. As a result, we use the static dielectric constant in our calculations. The system under investigation is asymmetric and does not necessarily suggest a continuum model, but continuum models have been applied successfully at surfaces in the past.[22,23] However, it is sensible to regard the values of P^+ calculated in this way as an upper limit to the actual value, because the C314 is also in contact with air ($\epsilon \sim 1$). We will show that this consideration has little qualitative effect on the conclusions.

For the CPCM calculations, we take the difference in energies between the neutral and cation species as the ionization energy, rather than relying on the Kohn−Sham orbital energies. We use geometries for the neutral and cationic forms of C314 optimized at the B3LYP/6-311+G(d,p) level of theory in the absence of a dielectric. The energies for both ion and neutral are then calculated using the CPCM model at the B3LYP/6-311+G(3df,2pd) level of theory. The change in zero-point energy calculated in the gas phase using the B3LYP/6-31G(d) level of theory is −0.001 eV. Our calculations neglect the change in zero point energy, though, as its value is very sensitive to the method of calculation. Nevertheless, our calculated ionization threshold for gas-phase C314 of 6.93 eV compares favorably to the measured vertical ionization potential of 7.10 eV from photoelectron spectroscopy.[25] In fact, by estimating the width of the feature centered at 7.10 eV in the photoelectron spectrum, we can estimate a threshold for ionization within 0.02 eV of our calculated value. There are many input parameters for the CPCM calculations, and most are more appropriate for molecular solvents than an ionic surface. However, the most important parameter is the dielectric constant. In practice, we choose the parameters to be consistent with chlorobenzene, a molecular solvent whose dielectric constant is similar to that of NaCl, and reassign the dielectric constant to be that of NaCl (5.9). The calculated ionization threshold for $\epsilon = 5.9$ is 5.58 eV, and the estimated value of P^+ is 5.58−6.93 = −1.35 eV.

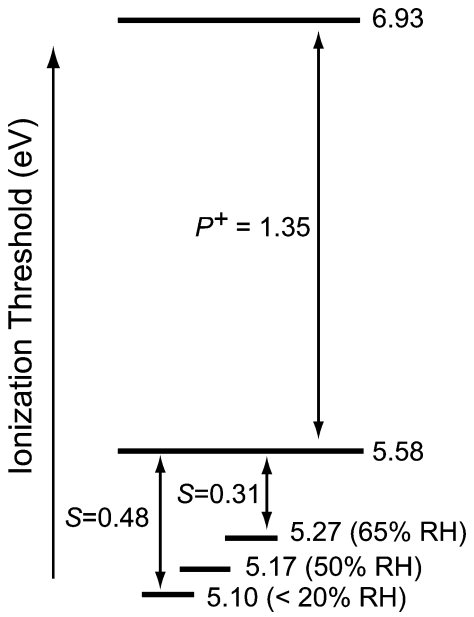

Figure 6. Energy level diagram showing the contributions of P^+ and S to the change in ionization threshold in going from the gas phase to the aerosol particle surface.

Comparing this result to other ionization threshold data shows that it is a reasonable result. The ionization threshold of perylene measured at the surface of liquid water is 0.9 eV lower than the gas-phase value ($P^+ = -0.9$ eV).[23] The effective dielectric constant for the water surface, which has been measured as 2.9,[23] is smaller than the value used here, so the stabilization energy is expected to be less than that for C314. Furthermore, perylene is nonpolar in both the neutral and the ion and, therefore, experiences no dipolar stabilization. Therefore, our result differs from this example in the expected way. The value of P^+ for water at the surface of water is −1.45 eV.[22] Although the effective dielectric constant of the water surface is, again, smaller than used in our calculation, the water molecule itself is much smaller than either C314 or perylene, enabling more efficient solvation and resulting in a larger value of P^+. Finally, the ionization threshold of several polycyclic aromatic hydrocarbons similar in size to C314 have been measured in a variety of bulk nonpolar fluids yielding values of P^+ that range from −1.0 to −1.5 eV.[15,19] Our calculated value of −1.35 eV, then, is within the expected range and consistent with other measured values. Finally, this value is the same as one would calculate with the Born equation using 4.45 Å as the cation radius, which is a physically reasonable number for C314.

From eq 2 it follows that S is −0.48 eV. Figure 6 is a graphical representation of the two contributions to the change in ionization threshold. Now that we have disentangled the relative contributions to the ionization threshold data, we can better understand the effect of adsorbed water.

Effective Dielectric Constants. As a zero-order approach, the polarization energy, P^+, can be estimated to be independent of the amount of adsorbed water on the surface. This interpretation is consistent with previous findings from AFM experiments[10] using scanning Maxwell stress microscopy (SMSM), a technique that can distinguish between surface potential and dielectric effects. The study shows preferential adsorption of water to step edges of a NaCl (001) surface in collection modes that are sensitive to changes in surface potential, but the

enhancement is not visible in the collection mode that is sensitive only to topography and the local dielectric. Thus, the adsorbed water has a much greater effect on the surface potential than on the local dielectric. Because P^+ is related to the dielectric constant, it should also be relatively unchanged by adsorbed water. In this limit, the change in threshold between RH < 5% and RH = 65% can be attributed predominantly to changes in *S*. The photoionization threshold increases from 5.10 to 5.27 eV over this range of RH, and the corresponding value of *S* changes from −0.48 to −0.31 eV.

As we have proposed above, adsorbed water can reduce the electric field experienced by C314 by producing structural changes in the underlying lattice and by producing an opposing field of its own. Though not directly indicative of the electronic properties of the adsorbed water itself, we can express the overall effect of the water in quantitative and concise fashion as an "effective" dielectric constant. In this limit, the ratio of the electric field magnitude experienced by the C314 in the absence of water to that in the presence of the water film yields the effective dielectric constant of the water film. Using the relationship for the Stark shift in ionization, $|S| \propto F^{1/2}$, we can generate an expression for the effective dielectric constant of the water films,

$$\epsilon_{\text{eff}} = \frac{F_{\text{dry}}}{F_{\text{wet}}} = \left(\frac{S_{\text{dry}}}{S_{\text{wet}}}\right)^2 \tag{3}$$

In this equation, *F* is the electric field magnitude and, as before, *S* is the ionization Stark shift. Applying eq 3 to the results produces the last column of data in Table 1. The dielectric constant grows from very near 1 at 20% relative humidity ($\Theta < 1$) to 2.4 at 65% relative humidity ($\Theta \sim 3$). If we consider the calculated value of P^+ to be an upper limit, the effective dielectric constants are also upper limits. A generous lower limit of $P^+ = -1.10$ eV changes the RH = 65% value to 1.7. In any case, a multilayer coverage of water dampens the effect of the electric field by approximately a factor of 2. The excited-state spectroscopy shows that C314 remains adsorbed to the surface at this value of RH. As a result, it may partially protect the underlying ions from the changes brought about by water.

Adsorption to Defect Sites. As was first described by Dent and Leonnard-Jones in 1928,[38] the defect-free NaCl lattice produces a strong electric field above the surface ions that perturbs the spectroscopy of adsorbed molecules.[39] C314 is large enough to span several lattice spacings, though. If the molecular plane of C314 lies parallel to the surface, one would expect efficient cancellations of the effects of the lattice, especially if the pertinent molecular orbitals are widely delocalized as expected. Therefore, the spectroscopy is unlikely to be representative of C314 adsorbed to the defect-free surface.

Another, more likely possibility is that C314 preferentially adsorbs to defect sites as does water. With the underlying symmetry broken, the net electric field produced by defects such as steps, edges, and vacancies can be very large. This interpretation explains the large red shift in the λ_{max} values relative to materials with similar dielectric constants. It is also consistent with the dependence of both λ_{max} and ionization threshold on RH. Because the majority of the changes in λ_{max} and IE occur for RH > 40% where the ionic mobility becomes much greater, it follows that these changes are correlated. Though the precise nature of these sites cannot be determined from these measurements, one can imagine a C314 molecule that is adsorbed to a step edge (or other defect) on the dry particle. When adsorbed water smoothes (or perhaps moves) the defect, the C314 is left on a flatter, effectively less-polar surface.

Using the λ_{max} value of ~335 nm for molecular solvents with $\epsilon \sim 5.9$ as a reference is a means of estimating the field magnitude experienced by C314 and making quantitative connections with the IE data. The electrochromic shift (in cm^{-1}) in the $S_1 \leftarrow S_0$ spectroscopy is given by

$$\Delta\tilde{E} = -\frac{F\Delta\mu\cos\gamma}{hc} \tag{4}$$

where *F* is the field magnitude, $\Delta\mu$ is the transition dipole moment magnitude, and γ is the angle between $\Delta\vec{\mu}$ and $\vec{F}$. Using 435 nm as the λ_{max} in the absence of a field and 448 nm as the value in the field, the electrochromic shift is 670 cm^{-1}. For $\gamma = 0$, eq 4 yields a lower limit on the corresponding value of *F* of 1×10^7 V/cm. The change in ionization threshold as a function of electric field has a different functional dependence on *F* and provides a check of internal consistency. An often used expression in ZEKE-PFI spectroscopy[34] of polyatomic molecules for the Stark shift in ionization threshold is

$$S = 4F^{1/2} \tag{5}$$

which is similar to the classical expression for the field ionization of Rydberg atoms. Here, the field is expressed in V/cm and *S* is in cm^{-1}. Although the linear dependence of *S* on $F^{1/2}$ is robust, the constant of proportionality varies among systems.[40] Also, the relationship is typically applied at much lower values of *F* ($0-10^4$ V/cm). Nevertheless, this equation predicts a shift of 1.6 eV, which is on the same order as our value of 0.48 eV. Because eq 5 is approximate, an order of magnitude agreement is satisfactory. Thus, both λ_{max} and IE measurements are consistent with a field magnitude on order 1×10^7 V/cm experienced by the C314.

As another consistency check for the value of *F* as well as our measured effective dielectric constants, we can use eq 4 to predict the value of λ_{max} at elevated RH. For RH = 65%, the value of ϵ_{eff} is 2.4, and replacing *F* with F/ϵ_{eff} in eq 4 predicts an electrochromic shift of 277 cm^{-1}. Again, using 435 nm as the zero-field reference for λ_{max}, the calculated λ_{max} for RH = 65% is 440 nm, which is close to our measured value of 441 nm. These data give strong evidence for electric fields on the order of 1×10^7 V/cm located on defect sites. Water reorganizes these sites, reducing the field experienced by the probe molecule by approximately a factor of 2 at RH = 65%.

The implications of these findings provide an interesting contrast to the existing data concerning the atmospheric chemistry of NaCl. The rates of many of the important reactions that take place on the NaCl surface increase as a function of water coverage.[4,41] In general, though, these reactions represent cases where the surface represents one of the reactants. Certainly, when the reaction involves the removal of chloride ions from the lattice, the ionic mobility is important. In these cases, adsorbed water greatly increases the ionic mobility and, thus, the reaction rate. Field studies show that a wide variety of organic molecules reside on sea salt aerosol particles.[13] Although the chemistry and photochemistry of these species is not characterized, the large fields present at NaCl surfaces can conceivably play a role. For example, the photocatalytic decomposition of several volatile organic compounds has been demonstrated on sea salt particles,[42] but the nature of these catalytic sites is unknown. Though the direct solvation by water of these adsorbed molecules will be important, an equally important consideration is the effect of water on the structure of the surfaces sites. Here, adsorbed water may decrease the catalytic activity of the surface by removing or altering the most

active sites. Furthermore, these results demonstrate the power of adsorbed water to alter the optical properties of species adsorbed to aerosol particles.

Summary

The excited-state absorption maximum of C314 adsorbed to NaCl aerosol particles is 448 nm with RH < 5%, which is red-shifted compared to materials with dielectric constants similar to NaCl. The interaction of C314 with the electric field produced by the lattice ions is responsible for the difference. Adsorbed water disrupts the effect of the electric field leading to a blue shift in the absorption spectrum of up to 7 nm at RH = 60%. Ionization threshold data show a similar trend, increasing from 5.10 to 5.27 eV over a similar range of RH, and this trend is also attributable to changes in the electric field experienced by C314. Both static dielectric effects of the water and changes in the surface topography at defect sites may contribute to changes in the field. A CPCM calculation separates the total solvent stabilization energy into two components: the polarization response of the surface (P^+) and the Stark shift owing to the electric field. This calculation allows an estimate of the effective dielectric constant of the adsorbed water film, which is approximately 2.4 for multilayer water coverages (RH = 65%). An important implication of these results is that the changes in the NaCl surface structure with adsorbed water have a drastic influence on the chemical environment of other adsorbed molecules.

Acknowledgment. We gratefully acknowledge grants from the Camille and Henry Foundation Faculty Start-up Awards Program and the Research Corporation Cottrell College Science Award. S.F.M. and C.N.W. thank the Camille and Henry Dreyfus Foundation for research stipends. E.W. thanks Research Corporation for summer support.

References and Notes

(1) Ellison, G. B.; Tuck, A. F.; Vaida, V. *J. Geophys. Res.-Atmos.* **1999**, *104*, 11633.
(2) Tervahattu, H.; Hartonen, K.; Kerminen, V. M.; Kupiainen, K.; Aarnio, P.; Koskentalo, T.; Tuck, A. F.; Vaida, V. *J. Geophys. Res.-Atmos.* **2002**, *107*.
(3) Weis, D. D.; Ewing, G. E. *J. Geophys. Res.-Atmos.* **1999**, *104*, 21275.
(4) Finlayson-Pitts, B. J.; Hemminger, J. C. *J. Phys. Chem. A* **2000**, *104*, 11463.
(5) Randles, C. A.; Russell, L. M.; Ramaswamy, V. *Geophys. Res. Lett.* **2004**, *31*.
(6) Cziczo, D. J.; Nowak, J. B.; Hu, J. H.; Abbatt, J. P. D. *J. Geophys. Res.-Atmos.* **1997**, *102*, 18843.
(7) Peters, S. J.; Ewing, G. E. *J. Phys. Chem. B* **1997**, *101*, 10880.
(8) Foster, M.; Ewing, G. E. *Surf. Sci.* **1999**, *428*, 102.
(9) Dai, Q.; Hu, J.; Salmeron, M. *J. Phys. Chem. B* **1997**, *101*, 1994.
(10) Luna, M.; Rieutord, F.; Melman, N. A.; Dai, Q.; Salmeron, M. *J. Phys. Chem. A* **1998**, *102*, 6793.
(11) Barraclough, P. B.; Hall, P. G. *Surf. Sci.* **1974**, *46*, 393.
(12) Engkvist, O.; Stone, A. J. *J. Chem. Phys.* **2000**, *112*, 6827.
(13) Cincinelli, A.; Stortini, A. M.; Perugini, M.; Checchini, L.; Lepri, L. *Marine Chem.* **2001**, *76*, 77.
(14) Reichardt, C. *Chem. Rev.* **1994**, *94*, 2319.
(15) Holroyd, R. A.; Preses, J. M.; Zevos, N. *J. Chem. Phys.* **1983**, *79*, 483.
(16) Saik, V. O.; Lipsky, S. *J. Phys. Chem.* **1994**, *98*, 11858.
(17) Hoffman, G. J.; Albrecht, A. C. *J. Phys. Chem.* **1991**, *95*, 2231.
(18) Hoffman, G. J.; Albrecht, A. C. *J. Phys. Chem.* **1990**, *94*, 4455.
(19) Casanovas, J.; Grob, R.; Delacroix, D.; Guelfucci, J. P.; Blanc, D. *J. Chem. Phys.* **1981**, *75*, 4661.
(20) Benderskii, A. V.; Eisenthal, K. B. *J. Phys. Chem. B* **2001**, *105*, 6698.
(21) Wang, H.; Borguet, E.; Eisenthal, K. B. *J. Phys. Chem. B* **1998**, *102*, 4927.
(22) Faubel, M.; Steiner, B.; Toennies, J. P. *J. Chem. Phys.* **1997**, *106*, 9013.
(23) Inoue, T.; Sasaki, S.-Y.; Tokeshi, M.; Ogawa, T. *Chem. Lett.* **1998**, 609.
(24) Ma, T.; Inoue, K.; Noma, H.; Yao, K.; Abe, E. *J. Mater. Sci. Lett.* **2002**, *21*, 1013.
(25) Kovac, B.; Novak, I. *Spectrochim. Acta Part a-Mol. Biomol. Spectrosc.* **2002**, *58*, 1483.
(26) Niessner, R. *J. Aerosol Sci.* **1986**, *17*, 705.
(27) Niessner, R.; Wilcox, C. F. *Anal. Chem.* **1989**, *61*, 708.
(28) Keller, A.; Fierz, M.; Siegmann, K.; Siegmann, H. C.; Filippov, A. *J. Vac. Sci. Technol. a-Vac. Surf. Films* **2001**, *19*, 1.
(29) Hueglin, C.; Paul, J.; Scherrer, L.; Siegmann, K. *J. Phys. Chem. B* **1997**, *101*, 9335.
(30) Mohr, M.; Burtscher, H. *J. Aerosol Sci.* **1997**, *28*, 613.
(31) Matter, D.; Mohr, M.; Fendel, W.; Schmidt-Ott, A.; Burtscher, H. *J. Aerosol Sci.* **1995**, *26*, 1101.
(32) Foster, M. C.; Ewing, G. E. *J. Chem. Phys.* **2000**, *112*, 6817.
(33) Hoffman, G. J.; Albrecht, A. C. *J. Phys. Chem.* **1991**, *95*, 2231.
(34) Muller-Dethlefs, K.; Schlag, E. W. *Annu. Rev. Phys. Chem.* **1991**, *42*, 109.
(35) Barone, V.; Cossi, M. *J. Phys. Chem. A* **1998**, *102*, 1995.
(36) Cossi, M.; Rega, N.; Scalmani, G.; Barone, V. *J. Comput. Chem.* **2003**, *24*, 669.
(37) Frisch, M. J.; G. W. T., Schlegel, H. B.; Scuseria, G. E.; Robb, M. A.; Cheeseman, J. R.; Montgomery, J. A., Jr.; Vreven, T.; Kudin, K. N.; Burant, J. C.; Millam, J. M.; Iyengar, S. S.; Tomasi, J.; Barone, V.; Mennucci, B.; Cossi, M.; Scalmani, G.; Rega, N.; Petersson, G. A.; Nakatsuji, H.; Hada, M.; Ehara, M.; Toyota, K.; Fukuda, R.; Hasegawa, J.; Ishida, M.; Nakajima, T.; Honda, Y.; Kitao, O.; Nakai, H.; Klene, M.; Li, X.; Knox, J. E.; Hratchian, H. P.; Cross, J. B.; Bakken, V.; Adamo, C.; Jaramillo, J.; Gomperts, R.; Stratmann, R. E.; Yazyev, O.; Austin, A. J.; Cammi, R.; Pomelli, C.; Ochterski, J. W.; Ayala, P. Y.; Morokuma, K.; Voth, G. A.; Salvador, P.; Dannenberg, J. J.; Zakrzewski, V. G.; Dapprich, S.; Daniels, A. D.; Strain, M. C.; Farkas, O.; Malick, D. K.; Rabuck, A. D.; Raghavachari, K.; Foresman, J. B.; Ortiz, J. V.; Cui, Q.; Baboul, A. G.; Clifford, S.; Cioslowski, J.; Stefanov, B. B.; Liu, G.; Liashenko, A.; Piskorz, P.; Komaromi, I.; Martin, R. L.; Fox, D. J.; Keith, T.; Al-Laham, M. A.; Peng, C. Y.; Nanayakkara, A.; Challacombe, M.; Gill, P. M. W.; Johnson, B.; Chen, W.; Wong, M. W.; Gonzalez, C.; Pople, J. A. *Gaussian 03*, revision B.05; Gaussian, Inc: Wallingford, CT, 2004.
(38) Lennard-Jones, J. E.; Dent, B. M. *Trans. Faraday Soc.* **1928**, *24*, 92.
(39) Dai, D. J.; Ewing, G. E. *J. Chem. Phys.* **1993**, *98*, 5050.
(40) Merkt, F.; Osterwalder, A.; Seiler, R.; Signorell, R.; Palm, H.; Schmutz, H.; Gunzinger, R. *J. Phys. B−At. Mol. Opt. Phys.* **1998**, *31*, 1705.
(41) Leu, M. T.; Timonen, R. S.; Keyser, L. F.; Yung, Y. L. *J. Phys. Chem.* **1995**, *99*, 13203.
(42) Isidorov, V.; Klokova, E.; Povarov, V.; Kolkova, S. *Catal. Today* **1997**, *39*, 233.